Low-Pressure DC Air Plasmas. Investigation of Neutral and Ion Chemistry

M. Castillo,[†] I. Méndez,[†] A. M. Islyaikin,[†,‡] V. J. Herrero,[†] and I. Tanarro[†,*]

Instituto de Estructura de la Materia (CSIC), Serrano 123, 28006 Madrid, Spain

Received: March 14, 2005; In Final Form: May 12, 2005

The neutral and charged species present in a direct current (dc) hollow cathode, gas flow, air reactor are experimentally studied by quadrupole mass spectrometry. The degree of ionization of the plasma and the electron mean temperature with decreasing air pressure, for constant discharge current, are measured with a double Langmuir probe. The chemical composition of the plasma changes appreciably over the 3×10^{-3} to 5×10^{-2} mbar range investigated: at the lowest pressures studied, O_2 dissociation is up to 60% and the concentration of NO is half that of N_2; concerning ions, NO^+ and N_2^+ are dominant for the whole pressure range. A kinetic model of the plasma including electrons, neutrals, and positive ions is developed to account for the experimental observations; it is consistent with energy balance and predicts that heterogeneous processes are the main source of NO and that the contribution of ions to the global chemistry of neutrals is of minor significance even for the lowest pressures.

Introduction

Low-pressure nonequilibrium plasmas of air and N_2/O_2 mixtures are currently attracting the attention of many scientific groups[1−7] due to their relevance in different fields, from the study of the Earth's ionosphere[8−14] to the reactivity in the boundaries of hypersonic vehicles[15] or the sterilization of surgical equipment.[16] Therefore, many efforts have been devoted to the experimental investigation and to the modeling[3,5,17−21] of these plasmas, characterized by gas temperatures close to 300 K (T_g < 0.05 eV) and comparatively high electron temperatures (T_e > 1 eV). Under these conditions, the collisions of energetic electrons with neutral precursors cause the formation of active species (atoms, radicals, ions, and excited molecules) that initiate the chemical reactions and lead to the appearance of other transients and secondary products.

Hollow cathode discharges (HCD) have a number of advantages over radio frequency (RF) and microwave (MW) reactors.[22,23] They provide a good geometrical resolution in positioning of different zones of the discharge. The easy control of the size and shape of discharge regions along with a suitable design of the reactor and adjustment of discharge conditions gives a great flexibility for many purposes.[24−29] In contrast with RF, MW discharges and the positive column of ordinary low-pressure dc discharges, HCDs have a negligible electric field in the enlarged negative glow region, which may be of interest in some specific studies, like those related with the chemistry of ionospheres.

Concerning the kinetic modeling of $N_2 + O_2$ and N_xO_y plasmas, more than 400 concurrent processes have been advanced in the literature;[5−19] nevertheless, the efforts made to identify the key processes and to reduce the number of reactions considered are generally welcomed, to construct more intelligible and manageable models.[30] In this respect, most three-body reactions can be disregarded at low pressures without noticeable changes in the predicted results.[31] Similarly, ions are usually neglected too in the chemistry of neutrals for pressures higher than 0.1−1 mbar,[32] due to very low ionization rates (<10^{-4}) in this kind of plasma. In any case, careful diagnostics of cold plasmas of these species at different pressures would be very convenient to identify and characterize the processes playing the key role for each pressure region.

In former works, the authors studied with time-resolved spectrometric techniques the neutral, atomic, and molecular species produced in modulated hollow cathode discharges of N_2O,[24,33,34] NO,[35] and NO_2,[36] at pressures ∼0.1−1 mbar and effective plasma volumes ∼0.02 L, verifying the formation of N_2 and O_2 as major products, and of minor proportions of the two nitrogen oxides other than the precursor in each case. Similarly, a discharge of natural air studied under conditions close to those of the N_xO_y plasmas[3] showed the formation of very small concentrations of NO and N_2O as compared with those of the N_2 and O_2 precursors. A simple kinetic model including electrons and neutrals, and the essential physicochemical processes, was also developed to explain the observed data. Most reaction rate constants, especially those for homogeneous reactions among neutrals, were taken from published databases.[37] Rate coefficients for many of the low-energy electron impact dissociation processes and for some of the heterogeneous reactions could be estimated from the time-resolved data.[3,36]

In the present work, we have extended the investigations with air plasmas to a much lower pressure range (down to 3×10^{-3} mbar) and have used a reactor100 times larger than that in the higher pressure study. Under these conditions of low collisionality, the electron temperature and the plasma ionization ratio are higher for a similar supply of electrical power and the relative importance of surface to gas-phase processes changes appreciably. As a result, the plasma chemistry is significantly modified. In the following, we describe the experimental characterization of these low-pressure air plasmas and use an improved version of the kinetic model, including ionic processes, to account for the chemical composition observed in the plasma and to estimate the relevance of the ions in the global plasma chemistry.

* Corresponding author. Fax: +34.91.5645557. E-mail address: itanarro@iem.cfmac.csic.es.

[†] Instituto de Estructura de la Materia (CSIC).

[‡] Present address: Dublin City University, School of Physical Sciences, Glasnevin, Dublin-9, Dublin, Ireland.

10.1021/jp051318m CCC: $30.25 © 2005 American Chemical Society
Published on Web 06/28/2005

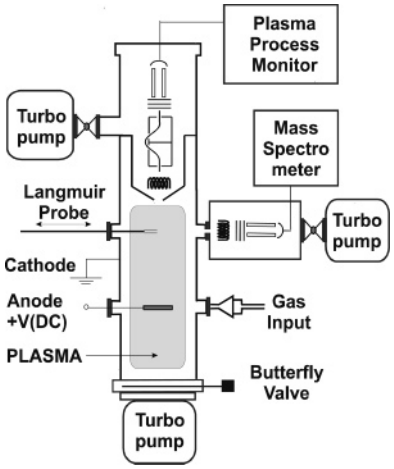

Figure 1. Experimental setup.

Experimental System

The experimental setup used for plasma generation and diagnostics is shown in Figure 1. A stainless steel dc glow discharge reactor, consisting basically of an enlarged hollow cathode cell with a grounded cylindrical vessel (10 cm diameter, 34 cm length) and a central anode, was used to achieve comparatively large plasma volumes. Differentially pumped quadrupole mass spectrometers for neutrals and ions and a double Langmuir probe were used for plasma diagnostics.

The reactor was continuously pumped by a 450 L/s turbomolecular pump to a background pressure of 10^{-6} mbar. A butterfly vacuum valve at the exit of the reactor, nearly closed during plasma operation, and a needle valve at the gas input allowed the pressure control of the discharge. Gas pressures in the range 3×10^{-3} to 5×10^{-2} mbar, measured with a capacitance manometer, were used for plasma generation. Residence times in the reactor were measured with discharge off, before and after each set of plasma measurements, by switching off quickly the air feed to the chamber and measuring the time evolution of the $m = 28$ amu mass spectrometric peak of N_2, using a digital oscilloscope. The results were always 2 s $\pm$20% for a fixed position of the butterfly valve at the exit of the reactor, independent of pressure, indicating in all cases a molecular gas flow regime. The measurement of residence times allowed an estimate of the different flow rate values, which were found to span the $\sim$0.4$-$7 sccm range for the different discharge pressures.

The reactor was electrically fed by a 0.2 A, 2000 V, dc source, through a 100 Ω ballast resistor. The maximum electric potential of the source was not high enough to turn on the discharge at the low operating pressures of the experiments; therefore, an electron gun built in the laboratory was used for ignition of the plasma. It consisted basically of a coiled tungsten filament (120 μm diameter, $\sim$3 Ω) heated by a 2 A, dc, $-$2000 V source, isolated of ground. Steady-state plasma currents $I_p \sim 150$ mA in the abnormal glow discharge conditions were maintained during the experiments.

The radial distribution of electron density and electron mean temperature in the cylindrical plasma volume were measured by means of a double Langmuir probe designed in our laboratory.[24] The approximation of orbital limited motion in a collision-free probe sheath for electropositive plasma was used.[35] The mass of the ions was approximated to a mean value of 30 amu for calculations of charge densities. A Maxwellian electron energy distribution was also supposed.

Molecular species were detected by means of an electron impact ionization quadrupole mass spectrometer, Balzers QMG112, working as residual gas analyzer, equipped with a Faraday cup detector. It was previously calibrated for the measurement of absolute concentrations of the individual gases of interest (N_2, O_2, NO, N_2O, NO_2).[35,36]

The measurement of ion fluxes was performed with a Plasma ProcessMonitor, Balzers PPM421, consisting of electrostatic focusing system, a cylindrical mirror energy analyzer (the upper limit was 510 eV) and a quadrupole mass spectrometer with a secondary electron multiplier in the counting mode. Both mass spectrometers were installed in independent vacuum chambers, communicating with the reactor by means of 200 and 100 μm holes, respectively. The chambers containing the mass spectrometers were differentially pumped down to 10^{-7} mbar by turbomolecular pumps backed by mechanical pumps. The ion flux ratio for each m/q^+ value was calculated by integrating its individual ion energy distribution. The relative sensitivity of the PPM 421 to different m/q^+ signals was calibrated by measuring its individual response in the detection mode of neutrals to known pressures of noble gases and hydrogen, supplied separately to the reactor chamber without discharge. The sensitivity of the secondary electron multiplier was calibrated too for the different ion masses by comparing its response (integrated in energy) to ions generated in discharges of the above-mentioned species, with that of a Faraday cup available as secondary detector in the plasma monitor. Both calibration methods led to a common sensitivity dependence for ions proportional to ($m^{-1/2}$), in agreement with former literature results,[39] except for the smallest m/q^+ value, where H^+ showed a slightly lower efficiency than H_2^+.

When the discharge was on, the signals of neutrals detected with the PPM421 plasma monitor decreased uniformly by a factor of 10 approximately, as compared with discharge off signals, probably due to space charge effects in the ionization region associated with direct flux of ions from the plasma; this effect prompted the use of the plasma monitor only to detect ions and the appliance of the QMG112 spectrometer for systematic detection of neutrals, because its sensitivity is not affected by the discharge.

The m/q^+ ratios of the energy integrated current signals for the different ionic species were transformed to relative ion densities in the plasma volume using the calibration dependences recorded beforehand. Absolute concentrations of ions (ions cm^{-3}) were obtained by scaling the total sum of the relative ion densities to the measured mean charge density.

Plasma Kinetics

The kinetic model used in this work is based on the numerical solution of a system of coupled differential equations accounting for the time evolution of various plasma species, from the ignition of the discharge until the attainment of its steady state. Stable molecules are considered to be homogeneously distributed throughout the reactor. Atoms, ions, and electrons are assumed to be confined to the negative glow with homogeneous concentrations. From the edge of this glow region, atoms diffuse and ions are accelerated toward the cathode wall through the plasma sheath. Throughout this work the gas temperature is assumed to be typically 298 K[24,28] and the electron energy distribution is approximated by a Maxwellian function characterized by a temperature T_e. Initial concentration of the precursors, gas flow rate, electron mean density, and electron temperature, all of them determined experimentally, are used as input parameters.

The present model is an extension of a former one initially developed to describe the behavior of the neutral species found

TABLE 1: Reactions Included in the Kinetic Model[a]

process	rate constant	γ	ref
Electron Impact Disocciation			
D_1: $N_2 + e^- \rightarrow 2N + e^-$	$1.0 \times 10^{-8} T_e^{1/2} e^{-16/T_e}$		42
D_2: $O_2 + e^- \rightarrow 2O + e^-$	$4.2 \times 10^{-9} e^{-5.56/T_e}$		41
D_3: $O_2 + e^- \rightarrow O + O(^1D) + e^-$	$5.0 \times 10^{-8} e^{-8.40/T_e}$		41
D_4: $NO + e^- \rightarrow N + O + e^-$	$7.4 \times 10^{-9} e^{-6.50/T_e}$		3
D_5: $N_2O + e^- \rightarrow N_2 + O + e^-$	$1.4 \times 10^{-9} e^{-1.67/T_e}$		3
D_6: $N_2O + e^- \rightarrow N_2 + O(^1D) + e^-$	$1.2 \times 10^{-9} e^{-3.64/T_e}$		3
D_7: $N_2O + e^- \rightarrow NO + N + e^-$	$1.0 \times 10^{-10} e^{-4.93/T_e}$		3
D_8: $NO_2 + e^- \rightarrow NO + O + e^-$	$5.6 \times 10^{-9} e^{-3.11/T_e}$		3
Electron Impact Ionization			
I_1: $N_2 + e^- \rightarrow N_2^+ + 2e^-$	$1.1 \times 10^{-8} T_e^{1/2} e^{-17.2/T_e}$		57
I_2: $O_2 + e^- \rightarrow O_2^+ + 2e^-$	$3.6 \times 10^{-9} T_e^{1/2} e^{-12.3/T_e}$		58
I_3: $N_2O + e^- \rightarrow N_2O^+ + 2e^-$	$1.4 \times 10^{-8} T_e^{1/2} e^{-12.9/T_e}$		59
I_4: $NO + e^- \rightarrow NO^+ + 2e^-$	$9.0 \times 10^{-9} T_e^{1/2} e^{-12.1/T_e}$		59
I_5: $NO_2 + e^- \rightarrow NO_2^+ + 2e^-$	$2.6 \times 10^{-9} T_e^{1/2} e^{-10.0/T_e}$		59
I_6: $NO_2 + e^- \rightarrow NO^+ + O + 2e^-$	$8.1 \times 10^{-9} T_e^{1/2} e^{-12.9/T_e}$		59
I_7: $O_2 + e^- \rightarrow O^+ + O + 2e^-$	$5.4 \times 10^{-10} T_e^{1/2} e^{-17/T_e}$		58
I_8: $N_2 + e^- \rightarrow N^+ + N + 2e^-$	$4.2 \times 10^{-10} T_e^{1/2} e^{-28/T_e}$		57
I_9: $N + e^- \rightarrow N^+ + 2e^-$	$1.0 \times 10^{-8}\ T_e^{1/2} e^{-14.5/T_e}$		60
I_{10}: $O + e^- \rightarrow O^+ + 2e^-$	$1.7 \times 10^{-8} T_e^{1/2} e^{-13.6/T_e}$		61
I_{11}: $NO + e^- \rightarrow O^+ + N + 2e^-$	$2.4 \times 10^{-9} T_e^{1/2} e^{-23/T_e}$		59
I_{12}: $NO + e^- \rightarrow O + N^+ + 2e^-$	$2.4 \times 10^{-9} T_e^{1/2} e^{-23/T_e}$		59
Electron Impact Neutralization			
N_1: $NO_2^+ + e^- \rightarrow NO + O$	$2.0 \times 10^{-7} (0.026/T_e)^{1/2}$		19
N_2: $N_2O^+ + e^- \rightarrow N_2 + O$	$2.0 \times 10^{-7} (0.026/T_e)^{1/2}$		19
N_3: $N_2^+ + e^- \rightarrow N + N$	$2.8 \times 10^{-7} (0.026/T_e)^{1/2}$		19
N_4: $O_2^+ + e^- \rightarrow O + O$	$2.0 \times 10^{-7} (0.026/T_e)$		19
N_5: $NO^+ + e^- \rightarrow N + O$	$4.0 \times 10^{-7} (0.026/T_e)^{3/2}$		19
Homogeneous Reactions			
G_1: $N + NO \rightarrow N_2 + O$	3.0×10^{-11}		37
G_2: $O + NO + M \rightarrow NO_2 + M$	1.0×10^{-31}		37
G_3: $O + NO_2 \rightarrow NO + O_2$	9.7×10^{-12}		37
G_4: $N + NO_2 \rightarrow N_2O + O$	1.2×10^{-11}		38
G_5: $O(^1D) + NO \rightarrow O_2 + N$	8.5×10^{-11}		37
G_6: $O(^1D) + N_2O \rightarrow 2NO$	7.2×10^{-11}		37
G_7: $O(^1D) + N_2O \rightarrow N_2 + O_2$	4.9×10^{-11}		38
G_8: $O(^1D) + NO_2 \rightarrow NO + O_2$	3.0×10^{-10}		37
Quenching of Excited States			
Q_1: $O(^1D) + NO \rightarrow O^3P + NO$	1.5×10^{-10}		37
Q_2: $O(^1D) + N_2 \rightarrow O^3P + N_2$	2.6×10^{-11}		37
Q_3: $O(^1D) + O_2 \rightarrow O^3P + O_2$	4.0×10^{-11}		38
Charge Transfer			
T_1: $N_2^+ + N_2O \rightarrow N_2O^+ + N_2$	5.0×10^{-10}		19
T_2: $N_2^+ + O_2 \rightarrow O_2^+ + N_2$	6.0×10^{-11}		19
T_3: $N_2^+ + O \rightarrow NO^+ + N$	1.3×10^{-10}		19
T_4: $N_2^+ + NO \rightarrow NO^+ + N_2$	3.3×10^{-10}		19
T_5: $N_2^+ + N_2O \rightarrow NO^+ + N_2 + N$	4.0×10^{-10}		19
T_6: $O_2^+ + N \rightarrow NO^+ + O$	1.2×10^{-10}		19
T_7: $O_2^+ + NO \rightarrow NO^+ + O_2$	4.4×10^{-10}		19
T_8: $O_2^+ + NO_2 \rightarrow NO_2^+ + O_2$	6.6×10^{-10}		19
T_9: $NO_2^+ + NO \rightarrow NO^+ + NO_2$	2.9×10^{-10}		19
T_{10}: $N_2O^+ + NO \rightarrow NO^+ + N_2O$	2.9×10^{-10}		19
T_{11}: $N^+ + O_2 \rightarrow N + O_2^+$	2.8×10^{-10}		19
T_{12}: $N^+ + O_2 \rightarrow NO^+ + O$	2.5×10^{-10}		19
T_{13}: $N^+ + O \rightarrow N + O^+$	10^{-12}		19
T_{14}: $N^+ + NO \rightarrow N + NO^+$	8×10^{-10}		19
T_{15}: $N^+ + O_2 \rightarrow O^+ + NO$	2.8×10^{-11}		19
T_{16}: $N^+ + NO \rightarrow N_2^+ + O$	3×10^{-12}		19
T_{17}: $N^+ + N_2O \rightarrow NO^+ + N_2$	5.5×10^{-10}		19
T_{18}: $O^+ + N_2 \rightarrow NO^+ + N$	1.18×10^{-12}		19
T_{19}: $O^+ + O_2 \rightarrow O_2^+ + O$	2×10^{-11}		19
T_{20}: $O^+ + NO \rightarrow NO^+ + O$	2.4×10^{-11}		19
T_{21}: $O^+ + NO \rightarrow O_2^+ + N$	3×10^{-12}		19
T_{22}: $O^+ + NO_2 \rightarrow NO_2^+ + O^3P$	1.6×10^{-9}		19
T_{23}: $O^+ + N_2O \rightarrow N_2O^+ + O$	4×10^{-10}		19
T_{24}: $O^+ + N_2O \rightarrow NO^+ + NO$	2.3×10^{-10}		19
T_{25}: $O^+ + N_2O \rightarrow O_2^+ + N_2$	2×10^{-11}		19
Wall Neutralization			
P_1: $N_2^+ + \text{wall} \rightarrow N_2$	eq 4		
P_2: $O_2^+ + \text{wall} \rightarrow O_2$	eq 4		
P_3: $NO^+ + \text{wall} \rightarrow NO$	eq 4		
P_4: $NO_2^+ + \text{wall} \rightarrow NO_2$	eq 4		
P_5: $N_2O^+ + \text{wall} \rightarrow N_2O$	eq 4		
P_6: $N^+ + \text{wall} \rightarrow N$	eq 4		
P_7: $O^+ + \text{wall} \rightarrow O$	eq 4		
Heterogeneous Reactions			
W_1: $O + \text{wall} \rightarrow O(s)$	$(0.011P + 1.4 \times 10^{-4})^{-1}$	1	31
W_2: $O + O(s) \rightarrow O_2$	29	4.2×10^{-3}	32
W_3: $N + \text{wall}\ (s) \rightarrow {}^1/_2 N_2$	2.6	0.07	54
W_4: $N + O(s) \rightarrow NO$	29	4.9×10^{-3}	32
W_5: $NO + O(s) \rightarrow NO_2$	0.01	2.0×10^{-6}	35
W_6: $N_2 + O(s) \rightarrow N_2O$	6.9×10^{-4}	1.3×10^{-7}	35
W_7: $O(^1D) + \text{wall} \rightarrow O$	$(0.011P + 1.4 \times 10^{-4})^{-1}$	1	33

[a] Rate coefficients are in units of cm^3 molecule^{-1} s^{-1} for electron impact and two-body homogeneous reactions; cm^6 molecule^{-2} s^{-1} for trimolecular reactions and s^{-1} for wall reactions. P is the pressure in mbar. T_e is the electron temperature in eV. O is $O(^3P)$ atom except when $O(^1D)$ or O(s) are indicated explicitly.

in dc and low-frequency modulated hollow cathode discharges of nitrogen oxides (N_2O, NO, NO_2)[33−36] and air,[3] at pressures in the ∼0.1−1 mbar range. These plasmas were generated in a reactor considerably smaller than that used here,[24] and with electrical charge densities up to 5×10^{10} cm^{-3}. The original model considered electron impact dissociation, two-body collisions between atoms and molecules, and heterogeneous reactions. It did not include ions, because the degrees of ionization of those plasmas were $\leq 10^{-5}$ and ions were not expected to influence appreciably the chemistry of neutrals.[31,32] In the present work, devoted to air discharges with much lower pressures but with similar charge densities, the ionization ratios are some orders of magnitude higher than before, and the influence of ions on the global chemistry cannot be disregarded a priori; therefore, ionic processes have been incorporated to the model. The new complete set of reactions is shown in Table 1.

Rate coefficients for low-energy electron impact dissociation of nitrogen oxides, unavailable previously in the literature,[40] were estimated in our previous studies from steady-state and time-resolved studies of dc discharges.[24,35,36] In analogy with the work of Lee et al.[41] on oxygen plasmas, an Arrehnius functionality, $k_D = A \exp(E_a/T_e)$, was assumed for the dependence of these coefficients with electron temperature (see discussion in ref 36). In our previous studies, electron impact dissociation of N_2 was always a minor channel and only an upper limit estimated from selected time-resolved measurements was considered.[3,36] In the present work, where electron temperatures can vary appreciably, an approximate Arrhenius dependence for the corresponding rate coefficient was derived from the electron impact dissociation cross sections of Cosby.[42] For the derivation of this rate coefficient, the measured cross sections for collision energies ≤50 eV were fitted to a rigid sphere line-of-centers model[43] with effective size πd^2 and threshold E_0. The corresponding rate constant is given by

$$k(T_e) = \pi d^2 \left(\frac{8T_e}{\pi\mu}\right)^{1/2} e^{-E_0/T_e} \qquad (1)$$

where T_e is the electron temperature in units of energy, and μ is the reduced mass of the colliding partners which, in this case, can be approximated by the mass of the electron. The resulting rate constant is expressed as D_1 in Table 1. The measurements of Cosby[42] suggest that predissociation to form $N(^2D) + N(^4S)$ is the most likely outcome of the collision process, but the contribution of the $N(^4S) + N(^4S)$ and $N(^2P) + N(^4S)$ channels

is also possible. For simplicity we have considered in the model only one kind of nitrogen atoms, labeled N, irrespective of their initial electronic state. This should not be a bad approximation, taking into account that the reactivity of $N(^2D)$ and $N(^2P)$ with the major molecular species present in the plasma is not too high.[44]

The gas-phase reactions of neutral species included in the model are the same as in previous works,[3] with identical expressions for the rate coefficients. Electron impact may also cause significant excitation of atoms and molecules.[17,45,46] The role of excited atoms and molecules in the kinetics of plasmas containing N_2 and O_2[47] was addressed in detail by Loureiro and co-workers (see refs 4, 5, and 48 and references therein), who showed that internal excitation can affect significantly the chemical composition of the plasma, specially at relatively high pressures (above 1 mbar).[4,17,49] However, the contribution of excited states for the present low-pressure plasmas is expected to be small and, except for the very reactive $O(^1D)$ atoms produced directly by O_2 electron impact dissociation, which has proven to play a key role in the kinetics of these plasmas,[3,34−36] nonexcited states have been considered.

Concerning heterogeneous reactions (W_i), we have used the same scheme as in our previous works. When the recombination probabilities are low enough to represent the limiting stage as compared to diffusion, the rate coefficients k_{W_i} have been estimated by taking into account the new reactor geometry and A/V ratio in the expression[31,50]

$$k_{W_i}[X_i]V = [X_i]\varpi_i\gamma_i A/4$$

$[X_i]$ is the concentration of each species and ϖ_i is its mean velocity at ambient temperature; A is the reactive wall area and V is the discharge volume. γ_i is the recombination probability per individual collision in the stainless steel surfaces for each process.

The recombination probabilities, γ_i, for N_xO_y formation (reactions W_4-W_6) on stainless steel, proposed as constant parameters, explained the observed appearance of N_2O in previous NO discharges and the formation of NO and N_2O in air plasmas,[35,36] and have not been modified in the present work.

Regarding the wall reactivity of oxygen, maximum probabilities for $O(^3P)$ adsorption (W_1) and $O(^1D)$ de-excitation (W_7) have been assumed (γ_1, $\gamma_7 = 1$), in agreement with refs 31 and 32. At the relatively high pressures (above 0.1 mbar) used in our previous works,[3,24,35,36] diffusion was the limiting process and W_1 and W_7 were inversely proportional to pressure, in agreement with Fick's law[51] and Chantry's model,[52] with a negligible dependence on γ_i. For the present discharge pressures, both diffusion and recombination in the wall contribute significantly. The joint contribution of the two processes can be expressed in terms of their respective characteristic times, $\tau_{total} = \tau_{diff} + \tau_{wall\ interaction}$, i.e.:

$$(k_{W_1},k_{W_7})_{total}^{-1} = \Lambda^2/d_i + (\varpi_O\gamma_{1,7}A/4V)^{-1}$$

where Λ is the characteristic diffusion length and d_i is the diffusion coefficient. Recent experimental values of the single step recombination probability of oxygen atoms on clean stainless steel ($O + \text{wall} \rightarrow O_2/2$) in a pure oxygen plasma have also been reported.[53,54] In our work, the recombination of O atoms in the wall is modeled as a two-step process through reactions W_1 and W_2 to contemplate simultaneously the recombination of oxygen atoms and the formation of nitrogen oxides, whose mechanisms are strongly entangled in our plasmas (see Table 1).

The recombination probability of nitrogen on the wall, γ_3, has been increased markedly from the previous model value,[3] in agreement with recent experimental data[54,55] obtained from pure N_2 discharges on clean stainless steel. Nevertheless, numerical predictions carried out carefully with the former and the present value show no difference for the present air plasmas, neither for the previous discharges of N_xO_y and air, because N_2 heterogeneous formation turns out to be a minor reaction channel as compared to gas-phase N_2 formation through reaction G_1.

Regarding ion processes, included presently to improve theoretical grounds of the measured concentrations of major ions, ionization by electron impact (I_1-I_{12}), recombination of electrons and positive ions ($N_1 - N_5$), two-body homogeneous reaction between ions and neutrals (T_1-T_{25}), and neutralization on the wall (P_1-P_7) are taken into account. Because electron density is assumed stationary from the very ignition of the discharge, electron multiplication by ionization processes should balance all types of electron loss, and to fulfill charge neutrality, ion composition at the ignition of the discharge is assumed to be N_2^+ and O_2^+ scaled to their respective parent molecules concentrations with $[N_2^+]_0 + [O_2^+]_0 = [e^-]$, their concentrations changing afterward by the kinetic processes (alternative tests with different N_2^+/O_2^+ initial ratios gave identical stationary ion distributions). The possible appearance of oxygen containing negative ions[19,41,56] has not been taken into account, because for the present T_e values, the main process of formation of O^- (the most abundant negative ion in O_2 plasmas), which is dissociative electron attachment to O_2, is roughly 1 order of magnitude less probable than O_2^+ production by electron impact, and because O^-, trapped in the negative glow, is very effectively neutralized by O^+ and O_2^+ or e^- impact (rate coefficients $>10^{-7}$ $cm^2\ s^{-1}$). Previous estimations found in the literature concerning pure O_2 glow discharges[41] provide ratios of O^- to electron densities $\sim 10^{-3}$ at O_2 partial pressures and electrical power surface densities equivalent to the present ones. Ozone, which is a common product of higher pressure air discharges, has not been detected in our plasma. In higher pressure discharges, three-body reactions involving oxygen atoms and molecules can lead to the formation of O_3, but these reactions are irrelevant under the present conditions. We are also not aware of the efficient process of O_3 generation on metallic surfaces. Apart from these possible sources, the formation of O_3 molecules in oxygen containing gas discharges results mainly from the following homogeneous reactions:

$$O^- + O_2(a^1\Delta_g) \rightarrow O_3 + e \quad k = 3.0 \times 10^{10}\ cm^{-3}\ s^{-1}\ \text{(ref 19)}$$

$$O_2^- + O(^3P) \rightarrow O_3 + e \quad k = 1.5 \times 10^{10}\ cm^{-3}\ s^{-1}\ \text{(ref 19)}$$

Therefore, the absence of O_3 supports further the present assumption of a low negative ion concentration.

Rate coefficients for electron impact ionization reactions (I_1-I_{12}) have been calculated from published experimental cross sections in the same way[43] as for electron impact dissociation of N_2 (D_4) (see eq 1 and Table 1), assuming a Maxwell electron energy distribution. Cross sections were expressed in analytic form by fitting the rigid sphere line-of-centers model to the low-energy regions of the available cross section data from refs 57−61. Alternative values for the ionization cross sections may be found in refs 41 and 62−66 and references therein. Discrepancies of the order of 25% are usually found among them. Cross sections for direct dissociative ionization of N_2, O_2, and NO

(reactions I_7, I_8, I_{11}, I_{12}) were not found in the literature. The available data[57−59] consist of global ionization cross sections through two or more join processes like

$$O_2 + e^- \rightarrow 2e^- + (O^+, O_2^{2+}) \text{ (ref 58)}$$

$$N_2 + e^- \rightarrow 2e^- + (N^+, N_2^{2+}) \text{ (ref 57)}$$

$$NO + e^- \rightarrow 2e^- + ((O^+ + N), (O + N^+)) \text{ (ref 59)}$$

As a result, the rate coefficients for reactions I_7 and I_8 to produce O^+ and N^+ have been obtained by fitting the "line-of-centers" to these two first dependences,[57,58] i.e., by neglecting the production of O_2^{2+} and N_2^{2+}, and those of I_{11} and I_{12} have been obtained by assigning one-half of the total cross section of ref 59 to each channel ($O^+ + N$) and ($O + N^+$). These rough approximations limit the precision of the predicted ions concentrations.

Rate coefficients for the recombination of electrons and positive ions (N_1-N_5), which depend on electron temperature, and those for homogeneous reaction between ions and neutrals (T_1-T_{25}) assuming the gas temperature of 300 K, have been taken from ref 19. Other data on ion−neutral reactions can be found in the compilations of Anicich (see ref 67 and references therein) and data for reactions N_3-N_5 are reported in ref 68, but they do not differ much from the data of ref 19. Several of these reactions involve only minor species in the present air plasmas, like N_2O or NO_2, but they may be significant in plasmas of nitrogen oxides. Three-body homogeneous reactions involving ion species are neglected.[3,36]

To calculate the wall loss rate coefficients, k_{P_n}, for each ionic species (processes P_1-P_7), a constant concentration of ions in the glow, equal to electron concentration, has been imposed. Therefore, net ion generation per time unit in the gas phase, assumed to be the difference between the total ionization through reactions I_1-I_{12} ($I_i = k_{I_i}[X_i][e^-]V_p$) and the total neutralization through reactions N_1-N_5 ($N_j = k_{N_j}[X_j^+][e^-]V_p$), must be compensated by the total ion flux to the cathode wall through processes P_1-P_7 ($P_n = k_{P_n}[X_n^+]V_p$), which represent the net contribution of positive charges, J, to the total electric current.

$$\sum_{n=1}^{7} P_n = \sum_{i=1}^{12} I_i - \sum_{i=1}^{5} N_j = \frac{J}{q^+} \qquad (2)$$

Ion mobility depends on the discharge conditions (plasma electric fields, electron and ion mean temperatures, reactor geometry, wall conditions, ...) which globally determine some plasma characteristics such as ambipolar diffusion or ion velocities at the sheath edge.[69] Nevertheless, these discharge conditions are the same for all ionic species and could be taken into account through a unique factor "β" independent of the ion identity. On the other hand, in agreement with the Child-Langmuir law, ion mobility is inversely proportional to the square root of the mass of each ionic species. The ratios between the individual P_n rate coefficients and ΣP_n ($n = 1-7$) are

$$\frac{P_n}{\sum_{n=1}^{7} P_n} = \frac{\beta[X_n^+]/\sqrt{m_n^+}}{\beta\sum_{n=1}^{7}[X_n^+]V_p/\sqrt{m_n^+}} = \frac{k_{P_n}[X_n^+]V_p}{\sum_{i=1}^{12} I_i - \sum_{i=1}^{5} N_j} \qquad (3)$$

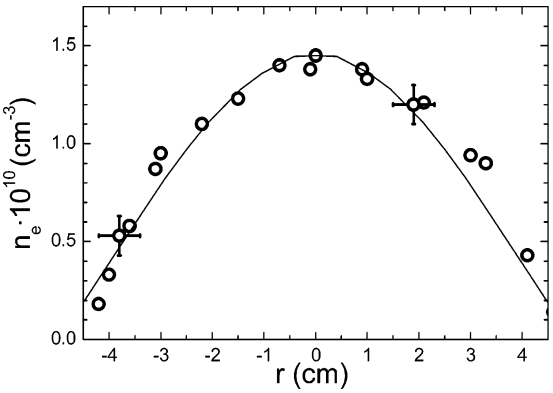

Figure 2. Experimental dependence of electron density, n_e, with radial position in the cylindrical hollow cathode reactor, r, measured with the double Langmuir probe (circles). Error bars indicate the uncertainties in the Langmuir probe results. Solid line: approximate theoretically predicted dependence of charge density with radial position, calculated as a zero-order Bessel function, $n_e(r) = n_e(0)\, J_0(2.405r/R)$, with $R =$ 5 cm (see text).

and the rate coefficients for neutralization in the wall, k_{P_n}, are given by the expression

$$k_{P_n} = \frac{\sum_{i=1}^{12} k_{I_i}[X_i^+][e^-] - \sum_{j=1}^{5} k_{N_j}[X_j^+][e^-]}{\sqrt{m_n^+}\sum_{n=1}^{7}[X_n^+]/\sqrt{m_n^+}} \qquad (4)$$

The rate constants, k_{P_n}, depend exponentially on T_e through the ionization coefficients k_{I_i} (and, to a much smaller extent, through k_{N_j}). Despite their markedly larger rate coefficients, ion neutralization in the gas phase turns out to be, in general, much less significant than ionization of neutrals by electron impact and ion loss in the wall and provides a minor contribution to the ion kinetics ($\leq$1%) for ionization ratios $\leq 10^{-3}$.[70] Charge-transfer reactions have not been included in equations[2−4] because they do not contribute to the net sink of electric charge density, because the chemical composition of ion flux bombarding the cathode surface was assumed not to change noticeably in the sheath zone due to very low gas pressure in the discharge chamber.

Results and Discussion

Figure 2 shows the radial distribution of electron density, n_e, obtained for a 140 mA, 4×10^{-3} mbar air discharge. It reaches maximum value at the symmetry axis ($\sim 1.5 \times 10^{10}$ cm^{-3}) and decreases toward the cathode wall. The mean electron temperature in the glow is approximately constant along the radius, within the experimental uncertainty ($\sim 4.2 \pm 0.4$ eV, for this pressure). The radial distribution of charge densities was measured at two different positions relative to the symmetry axis of the reactor, ~15 cm apart one from each other and one of them at the anode height, supplying identical results. The radial resolution of the measurements is limited by the 8 mm active length of the Langmuir probe (see Figure 1). Uncertainties in n_e are mainly due to electrical noise in the characteristic curve of the double Langmuir probe. These charge distributions were very similar for all discharge pressures in the range 0.003−0.05 mbar; their mean value, $[e^-] = 10^{10}$ cm^{-3}, was assumed to be the electron density in the "zero-order dimensional" kinetic model.[41,31,32] The solid line in Figure 2 displays a zero-order Bessel function scaled to the maximum electron density at the

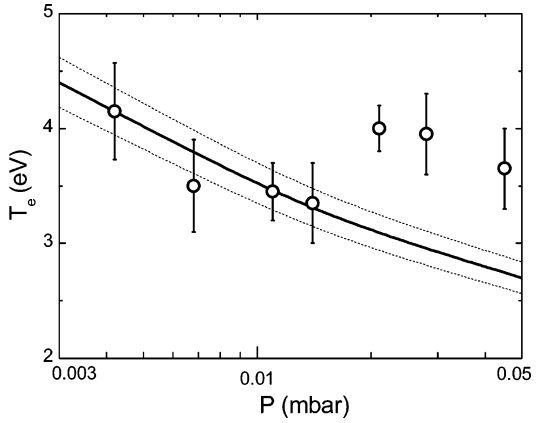

Figure 3. Dependence of electron mean temperature with gas pressure on a 140 mA air discharge. (circles) Experimental data with bar uncertainties from Langmuir probe. (solid line) Theoretical predictions, assuming that cathode current is completely due to ions; dashed lines display the T_e predicted variations justifying a change in discharge current up to 20%.

discharge axis and to the reactor radius ($R = 5$ cm). Assuming that the ion mean free path and sheath thickness are both small as compared to R, this function would correspond to the approximate steady-state solution for charge density in a cylindrical discharge at the "high-pressure" diffusion limit.[69]

Figure 3 shows the dependence of electron mean temperature, T_e, on the gas pressure. Circles, with error bars, are the experimental data measured with the Langmuir probe, for the discharge current $J = 140$ mA. The solid line corresponds to the T_e needed to reproduce the experimental current (approximated as the cathodic ion current) with the kinetic model:

$$\sum_{n=1}^{7} P_n = \frac{J}{q^+} = (140\ mA/q^+) \qquad (5)$$

Note that the current is strongly dependent on T_e; a 5% reduction in T_e leads to a decrease in the ion current larger than 20%. It is known that it is impossible for ions to carry absolutely all the current in the cathode sheath, because secondary electrons, created by ion impact at the cathode, are required to sustain the discharge.[69] The neglect of the secondary electron current implicit in eq 5 would thus be within a reasonable uncertainty in the model estimate for T_e (dashed lines in Figure 3). This uncertainty can justify the appearance of secondary electrons, not included in the model, as well as the power balance of the discharge (see below). Besides, the selection of ionization cross section values different from those of Table 1 to adjust the I_i rate coefficients by the "line-of-centers" model would modify J values calculated with a given T_e. For example, a 15% decrease in the ionization cross section of NO (reaction I_4), which is just the uncertainty given in ref 59 for the values, would lead to a reduction in the total ion current up to 10% for a fixed T_e value, and even larger uncertainties can be found by comparing the different bibliographic data sources (where ionization cross section discrepancies surpass 50%). On the other hand, the agreement between the T_e measurements and model predictions is within experimental uncertainty at the lower pressures and is worse at the higher ones. With increasing pressure, as the ionization degree decreases, a worse approximation of the electron energy distribution function to a Maxwellian might explain the observed discrepancies;[71] besides, an already noticeable concentration of negative ions, mainly O^-, not included in the model, might begin to appear. Because the condition of

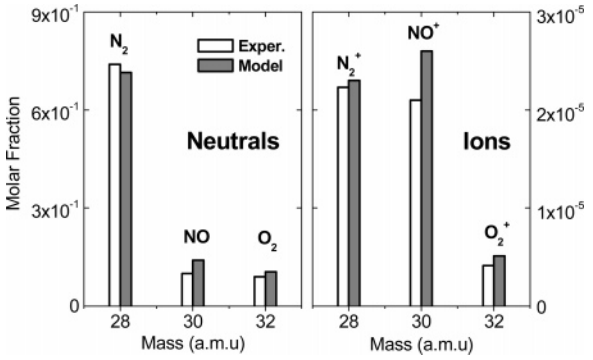

Figure 4. Bar-graph partial mass spectra of experimental molar fractions and model predictions displaying the three major neutrals and ions, obtained in a 140 mA, 0.0065 mbar, 1 sccm, air discharge.

charge neutrality holds for quasi-neutral plasmas, if the negative ion density increases, the electron density should go down. In this case, the overall ionization rate would also decrease and the electron temperature should increase to compensate it.[41,56]

Figure 4 displays molar fractions of the major three neutrals (left panel) and ions (right panel) recorded in our experiments (gray bars) and predicted by the model (white bars). These data were obtained for a 140 mA, 0.0065 mbar, air discharge. The relative ion fluxes, J_i, calculated by integrating individually the m_i/q^+ ion energy distributions detected by the plasma monitor, were scaled to absolute densities in the glow by using the Child−Langmuir law and normalizing to the mean electron density.

$$\sum_i J_i \sqrt{m_i} = [n_e^-]$$

Maximum contributions from the sum of minor neutral and ion products to these signals are less than 5%. The similarity of the NO concentration to that of O_2 and a NO^+ molar fraction comparable to that of N_2^+ (and much higher than that of O_2^+) are the most remarkable results. A reasonable agreement between measured and calculated data is found at this pressure.

Figure 5 displays the theoretical predictions for concentrations of all gas species included in the model as a function of discharge pressure, at constant gas residence time (2 s), charge density ($[e^-] = 10^{10}$ cm^{-3}), and electric current (140 mA). The theoretical predictions correspond to a 5 s delay from the ignition of the discharge, corresponding to the steady state, which is reached in a time ≤ 2 s. The upper panel shows the neutral species and the lower panel displays the ions. Contrary to N_2 and O_2, which decrease close to linearly with pressure, a nearly constant NO concentration is estimated, so that NO exceeds largely the O_2 concentration at the lowest pressures and reaches almost half the concentration of N_2. The predicted concentrations of N_2O and NO_2 molecules are at least 1 order of magnitude lower than those of N_2, O_2, and NO over all the pressure range and show opposite behavior with pressure. With the aim to elucidate the influence of ions in the concentration of neutral species, the kinetic model was also run after canceling the processes involving ions. Identical predictions were obtained for neutrals to those displayed in Figure 5, proving that ions can be neglected in the chemistry of neutrals, even at the lowest pressures studied. Conversely, recent detailed simulations of the former air and N_xO_y discharges[3,24,35,36] at higher pressures with the presently improved model led to analogous predictions to those previously calculated.

Figure 6 shows the pressure dependent molar fractions of the three major neutral and ion species for the conditions of Figure 5, as obtained experimentally (symbols) and simulated

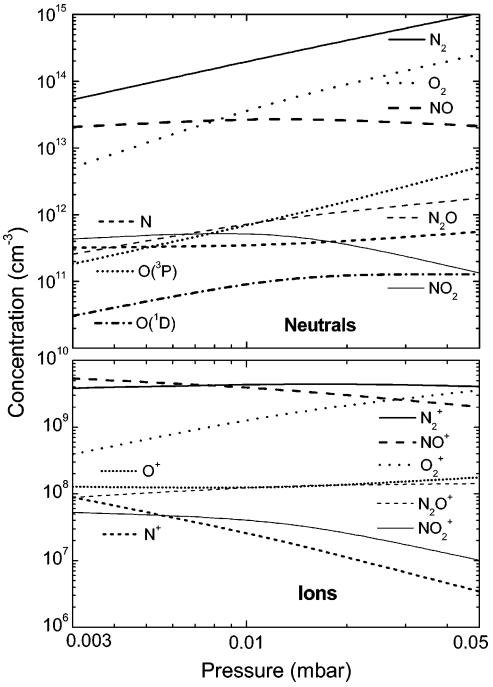

Figure 5. Model predictions for the dependence of neutral and ion concentrations on pressure for air discharges, for constant electric current (140 mA) and gas residence time (2 s). Gas flow rates increase linearly with pressure between 0.43 sccm at 0.003 mbar and 7.3 sccm at 0.05 mbar.

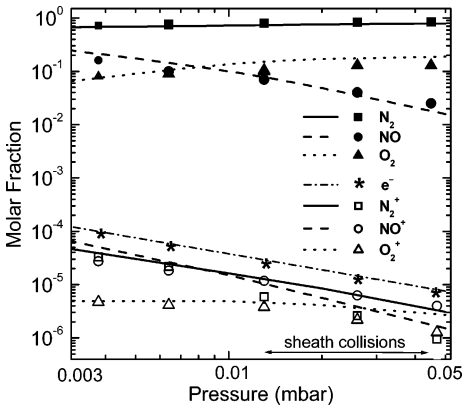

Figure 6. Experimental (symbols) and simulated (lines) molar fraction dependences on pressure of the major molecules and ions in the present air discharges. The size of the symbols indicates approximately the experimental uncertainties.

with the model (lines). This presentation is convenient to stress the variation of the plasma ionization ratio with discharge pressure for a constant electron density, $[e^-] = 10^{10}$ cm^{-3}. The variation in the relative concentration of the major precursor N_2 is very small (~10%). In contrast with N_2, the degree of dissociation of O_2 grows with decreasing pressure, reaching ~60% and promoting heterogeneous NO formation. As can be seen, the agreement between experimental and theoretical results is very encouraging for neutrals. Note that, neither the simple scheme of heterogeneous reactions leading to O_2 recombination and NO formation, deduced in our previous works on nitrogen oxide plasmas, nor the corresponding γ_i probabilities, have been modified in the present work, in which heterogeneous NO formation is much more important.

Concerning ions, a good agreement is found for the lower pressures, where N_2^+ and NO^+ reach similar concentrations, and O_2^+ is approximately 1 order of magnitude less abundant.

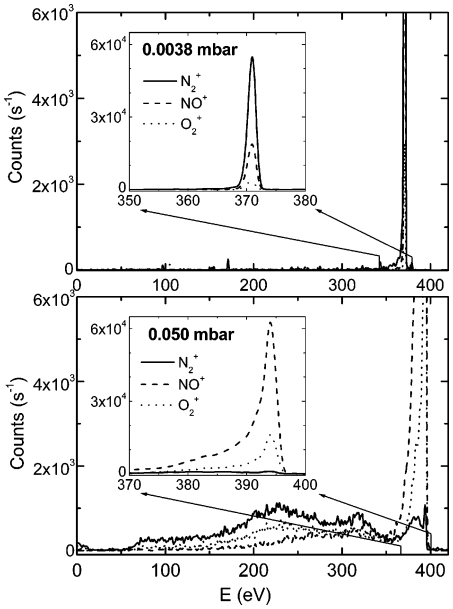

Figure 7. Energy distribution of major ions for 0.0038 mbar (upper panel) and 0.050 mbar (lower panel), 140 ± 5 mA, hollow cathode air discharges.

At higher pressures, the agreement is not so good, because the experimental results display a slight predominance of NO^+ above N_2^+ and O_2^+, in contrast to the theoretical predictions. A simulation at these pressures with higher T_e values, matching the experimental ones, did not solve this disagreement. A possible qualitative explanation of this discrepancy might be the appearance of collisions in the cathode sheath with increasing pressure, not taken into account in the theoretical model. As an indication of this possibility, Figure 7 shows the different ion energy distributions of N_2^+, O_2^+, and NO^+ ions reaching the cathode at 0.0038 mbar (upper panel) and 0.050 mbar (lower panel). The insets display the regions around the maxima. For 0.0038 mbar, very sharp peaks at 371 eV can be seen (fwhm ~2 eV) and a negligible noise contribution appears at low energies. It indicates that ions reaching the sheath from the glow accelerate and reach the cathode surface without collisions. On the contrary, broader maxima appear at 0.05 mbar discharge pressure, with a significant widespread background reaching low ion energies, mainly for N_2^+. This points to collisions between ions and neutrals in the sheath, either of elastic or with charge transfer nature.

A precise calculation of the power balance of the present discharges is out of the scope of this work and only an approximate evaluation will be given. The 0.0038 mbar air discharge, whose cathode ion energy distribution is shown in the upper panel of Figure 7, corresponds to the particular case of a 140 ± 5 mA discharge, with 376 ± 1 V anode−cathode potential; therefore, the total power supplied to the reactor in this case is $W_T = 52.6 \pm 2.0$ W. The minimum power spent in dissociation and ionization processes can be estimated theoretically by taking into account each individual process in the steady state and assuming that, at least, an energy contribution equal to its threshold is needed. Although many of these processes will take place at electron energies higher than threshold, this rough evaluation predicts that total dissociation and ionization reactions need at least power supplies of $W_D = 7.3$ W and $W_I = 2.4$ W respectively, to sustain the plasma. In addition, electrons carry a part of the energy to the anode and, for Maxwellian electrons, the mean energy lost per electron is $2T_e$.[69] Under the conditions of the present experiment, with $T_e = 4.2$

eV, this means an electron power loss of $W_e = 1.2$ W in the anode. On the other hand, it is known that most of the power consumption in dc plasmas is used to accelerate positive ions in the sheath region, which ultimately collide with the cathode surface, dissipating their kinetic energy as heat. The "sheath collision free" ion energy distributions of Figure 7, upper panel, show sharp maxima at 371 eV, very close to the 376 V anode−cathode potential. This indicates that the power supplied by an ion current of 140 mA to the cathode would be $W_C = 51.9$ W. Therefore, only $W_T - W_C = 0.7$ W of the total power supplied to the discharge would be used in the plasma chemistry of the negative glow, a value much lower than that predicted by the kinetic model: $W_D + W_I + W_e \geq 10.9$ W. This apparent contradiction has been commented on previously in the literature[69,72] and is justified by the emission of secondary electrons by the cathode walls under the impact of energetic ions and excited neutrals. The secondary electron emission coefficients depend on the material and surface conditions of the electrode, the energy and nature of impinging particles,[73−75] but the emission ratio usually does not exceed ∼0.1−0.2 for ions with kinetic energies lower than 500 eV. To estimate the electron mean temperature necessary to sustain a 140 mA discharge (continuous line in Figure 3), it was assumed that positive ions bombarding the cathode walls were the only electric charges responsible for the cathode current; nevertheless, a decrease in T_e as small as 5%, shown as the lower dashed line in Figure 3, is enough to justify a 20% decrease in ion current and the power balance, due to the dependence, $\sim e^{-E/T_e}$, of the ionization coefficients as mentioned above. The decrease in T_e is smaller than the experimental uncertainty of the Langmuir probe results, and smaller than the imprecision in the calculated current caused by the bibliographic discrepancies on ionization cross sections by electron impact.

Summary and Conclusions

A characterization of dc, low-pressure, hollow cathode air discharges by mass spectrometry of neutral and ion species, and by a double Langmuir probe, has been made. The experimental data have been compared with the predictions of a simple kinetic model, developed in previous works to study the neutrals produced in plasmas of nitrogen oxides and air, which has been improved presently to include the ion kinetics. The comparison between experimental and theoretical results provides a valuable insight into the relevance of the different plasma processes, the interaction between neutral and charged species, the behavior of electron energy, and the role of the reactor walls. Experimental studies on thermal nonequilibrium air and N_2/O_2 plasmas reported in the literature have been usually performed under very different physical conditions. The pressure range selected for this study (3×10^{-3} to 5×10^{-2} mbar) allows the observation of strong variations in the relative concentration of the major neutral and ionic species. The kinetic model can justify these variations and helps identify the key processes determining the global plasma chemistry. It should be stressed again at this point that the model, though simple, can account for the essentials of the cold plasma chemistry of oxygen, nitrogen, and nitrogen oxides discharges over a wide range of physicochemical conditions, including a change of nearly 4 orders of magnitude in pressure. Further improvements in the model like the incorporation of internally excited species other than $O(^1D)$, or a more rigorous treatment of the electron energy distribution might be considered in the future, but in its present state, the model is already very useful for the discrimination between key and peripheral processes, as indicated in the following paragraphs.

A dissociation of O_2 up to 60% at lowest pressures, in comparison with its discharge off concentration, and a remarkable formation of NO were observed. The N_2 concentration decrease is less important but reaches up to 10% at 3×10^{-3}mbar. On the other hand, NO^+ is the major positively charged species, even surpassing the N_2^+ density.

NO formation in the discharge is attributed to the heterogeneous reaction of N with O adsorbed on the stainless steel cathode surfaces. This assumption justifies suitably the increase in NO concentration with decreasing pressure experimentally observed. Moreover, the agreement between the present data and previous measurements performed for air or N_xO_y discharges at pressures 2 orders of magnitude higher than the present ones, with very different cathode dimensions,[3,35−36] lends support to this assumption and to the heterogeneous recombination probabilities proposed. Notwithstanding, homogeneous reactions of excited states leading to NO could be distinguishable in plasmas where the wall effects were less efficient.

The NO^+ predominance among positive ions at low pressures is mainly due to the high NO ionization coefficient by electron impact, which is considerably larger than those of O_2 and N_2 for the present T_e values. Nevertheless, charge-transfer reactions represent a noticeable contribution to NO^+ production at the highest discharge pressures and lowest T_e values, where the most effective charge-transfer processes, T_4 and T_7, produce up to ∼60% of total NO^+ at 0.05 mbar.

The model calculations of the densities of neutrals performed with and without ions show hardly any difference, even at pressures down to $\sim 10^{-3}$ mbar. Therefore, the irrelevance of ions in the kinetics of neutral species is confirmed. The electron mean temperatures estimated from the model for the measured current grow with decreasing pressure and are consistent with power balance within the uncertainty of the data.

Acknowledgment. The technical advice of J. M. Castillo, M. A. Moreno, and J. Rodríguez has been most valuable for the achievement of the present results. The SEUID of Spain (Projects FIS2004-00456, FTN2003-08228-C03-03) and C.A.M. (07N/0058/2002) are gratefully acknowledged for financial support.

References and Notes

(1) de Benedictis, S.; Dilecce, G. *J. Phys. III* **1996**, *6*, 1189.
(2) Cartry. G.; Magne, L.; Cernogora, G. *J. Phys. D: Appl. Phys.* **1999**, *32*, 1894.
(3) Castillo, M.; Herrero, V. J.; Méndez, I.; Tanarro, I. *Plasma Sources Sci. Technol.* **2004**, *13*, 343.
(4) Guerra, V.; Loureiro, J. *Plasma Sources Sci. Technol.* **1997**, *6*, 373
(5) Nahorny, J.; Ferreira, C. M.; Gordiets, B.; Pagnon, D.; Touzeau, M.; Vialle, M. *J. Phys. D: Appl. Phys.* **1995**, *28*, 738.
(6) Selvin, P. C.; Iwase, K.; Fujii, T. *J. Phys. D: Appl. Phys.* **2002**, *35*, 675.
(7) Smith, M. A. *Int. Rev. Phys. Chem.* **1998**, *17*, 35.
(8) Bilitza, D.; Rawer, K.; Bossy, L.; Gulyaeva, T. *Adv. Space Res.* **1993**, *13*, 15−23
(9) Bilitza, D. *Adv. Space Res.* **1998**, *21*, 871.
(10) Diloy, P. Y.; Robineau, A.; Lilensten, J.; Blelly P. L.; Fontanari, J. *Ann. Geophys.* **1996**, *14*, 191.
(11) Friedrich, M.; Torkar, K. M. *Adv. Space Res.* **1998**, *22*, 157.
(12) Stubbe, P.; Hagfors, T. *Surveys Geophys.* **1997**, *18*, 57.
(13) Wayne, R. P. *Chemistry of Atmospheres*; Oxford University Press: Oxford, NY, 2000.
(14) Zipf, E. C.; Prasad, S. S. *Nature* **1980**, *287*, 525.
(15) Capitelly, M. *Molecular Physics and Hypersonic Flows*; NATO-ASI Series Vol. C-482; Kluwer Academic Publishers: Dordrecht, The Netherlands, 1996.
(16) Moisan, M.; Barbeau, J.; Moreau, S.; Pelletier, J.; Tabrizian, M.; Yahia, L. H. *Int. J. Pharmaceut.* **2001**, *226*, 1.
(17) Gordiets, B.; Ricard, A. *Plasma Sources Sci. Technol.* **1993**, *2*, 158.
(18) Gordiets, B.; Ferreira, C. M.; Nahorny, J.; Pagnon, D.; Touzeau, M.; Vialle, M. *J. Phys. D: Appl. Phys*. **1996**, *29*, 1021.

(19) Kossyi, I. A.; Kosstinsky, Y.; Matveyev, A. A.; Silakov, V. *Plasma Sources Sci. Technol.* **1992**, *1*, 207.
(20) Sieck, L. W.; Heron, J. T.; Green, D. S. *Plasma Chem. Plasma Processing* **2000**, *20*, 235.
(21) Stefanovic, I.; Bibinov, N. K.; Deryugin, A. A.; Vinogradov, I. P.; Napartovich, A. P.; Wiesemann, K. *Plasma Sources Sci. Technol.* **2001**, *10*, 406.
(22) de la Cal, E.; Tafalla, D.; Tabarés, F, L. *J. Appl. Phys.* **1993**, *73*, 948.
(23) Hellmich, A.; Jung, T.; Kielhorn, A.; Rissland, M. *Surf. Coating Techol.* **1998**, *98*, 1541.
(24) de los Arcos, T.; Domingo, C.; Herrero, V. J.; Sanz, M. M.; Shulz, A.; Tanarro, I. *J. Phys. Chem. A* **1998**, *102*, 6282.
(25) Sanz, M. M.; Abad, L.; Herrero, V. J.; Tanarro, I. *J. Appl. Phys.* **1992**, *71*, 5372.
(26) Tabarés, F. L.; Tafalla, D.; Tanarro, I.; Herrero, V. J.; Islyaikin, A.; Maffiotte, C. *Plasma Phys., Controlled Fusion* **2002**, *44*, L37.
(27) Tabarés, F. L.; Tafalla, D.; Tanarro, I.; Herrero, V. J.; Islyaikin, A. M. *Vacuum* **2004**, *73*, 161.
(28) Tanarro, I.; Sanz, M. M.; Bermejo, D.; Domingo, C.; Santos, J.; Domenech, J. L. *J. Phys. Chem.* **1994**, *98*, 5862.
(29) Tanarro, I.; Arcos, T.; Domingo, C.; Herrero, V. J.; Sanz, M. M. *Vacuum* **2002**, *64*, 457.
(30) Hempel, F.; Davies, P. B.; Loffhagen, D.; Mechold, L.; Röpcke, J. *Plasma Sources Sci. Technol.* **2003**, *12*, S98.
(31) Cleland, T. A.; Hess, D. W. *J. Electrochem. Soc.* **1989**, *136*, 3103.
(32) Kline, L. E.; Partlow, W. D.; Young, R. M.; Mitchell, R. R.; Congedo, T. V. *IEEE Trans. Plasma Sci.* **1991**, *19*, 278.
(33) de los Arcos, T.; Domingo, C.; Herrero, V. J.; Sanz, M. M.; Schulz, A.; Tanarro, I. *J. Phys. Chem. A* **2000**, *104*, 3974.
(34) de los Arcos, T.; Castillo, M.; Domingo, C.; Herrero, V. J.; Sanz, M. M.; Tanarro, I. *J. Phys. Chem. A* **2000**, *104*, 8183.
(35) Castillo, M.; Herrero, V. J.; Tanarro, I. *Plasma Sources Sci. Technol.* **2002**, *11*, 368.
(36) Castillo, M.; Herrero, V. J.; Méndez, I.; Tanarro, I. *Plasma Sources Sci. Technol.* **2004**, *13*, 39.
(37) Atkinson, R.; Baulch, D. L.; Cox, R. A.; Hampson, Jr. R. F.; Kerr, J. A.; Rossi, M. J.; Troe, J. *J. Phys. Chem. Ref. Data* **1999**, *28*, 191.
(38) Wesley, F.; Herron, J. T.; Hampson, R. F.; Mallard, W. G. Eds. *NIST Chemical Kinetics Database*; U.S. Department of Comerce: Gaithersburg, MD, 1992.
(39) Okada, K..; Komatsu, S. *J. Appl. Phys.* **1998**, *84*, 6923.
(40) *Database Needs for Modeling and Simulation of Plasma Processing*, Nat. Res. Council, National Academy Press: Washington, DC, 1996.
(41) Lee, C.; Graves, D. B.; Lieberman, M. A.; Hess, D. W. *J. Electrochem. Soc.* **1994**, *141*, 1546.
(42) Cosby, P. C. *J. Chem. Phys.* **1993**, *98*, 9544.
(43) Steinfeld, J. I.; Francisco, J. S.; Hase, W. L. *Chemical kinetics and dynamics*; Prentice Hall: Englewood Cliffs, NJ, 1999.
(44) Herron, J. T. *J. Phys. Chem. Ref. Data.* **1999**, *5*, 1453.
(45) Jones, D. B.; Campbell, L.; Bottema, R. L.; Belic, D. S. *New J. Phys.* **1996**, *5*, 114.
(46) Vicic, M.; Poparic, G.; Belic, D. S. *J Phys B: At. Mol. Opt Phys.* **1996**, *29*, 1273.
(47) Polak, L. S.; Lebedev, Yu A. Eds. *Plasma Chemistry*; Cambridge International Science Publishers: Cambridge, U.K., 1998.
(48) Guerra, V.; Pinheiro, M. J.; Gordiets, B. F.; Loureiro, J.; Ferreira, C. M. *Plasma Sources Sci. Technol.* **1997**, *6*, 220.
(49) Guerra, V.; Galiaskarov, E.; Loureiro, *J. Chem. Phys. Lett.* **2003**, *371*, 576.
(50) Sabadil, H.; Pfau, S. *Plasma Chem. Plasma Processing* **1985**, *5*, 67
(51) Levine, I. R. *Physical Chemistry*; McGraw-Hill: New York, 1978.
(52) Chantry, P. J. *J. Appl. Phys.* **1987**, *62*, 1141.
(53) Gomez, S.; Steen, P. G.; Graham, W. G. *Appl. Phys. Lett.* **2002**, *81*, 19.
(54) Singh, H.; Coburn, J. W.; Graves, D. B. *J. Appl. Phys.* **2000**, *88*, 3748.
(55) Adams, S. F.; Millar, T. A. *Plasma Sources Sci. Technol.* **2000**, 9, 248
(56) Lee, C.; Lieberman, M. A. *J. Vac. Sci. Technol. A* **1995**, *13*, 368.
(57) Krishnakumar, E.; Srivastava, S. K. *J. Phys. B* **1993**, *23*, 1893.
(58) Krishnakumar, E.; Srivastava, S. K. *Int. J. Mass Spectrom. Ion Processes* **1992**, *113*, 1.
(59) López, J.; Tarnovsky, V.; Gutkin, M.; Becker, K. *Int. J. Mass. Spectrom.* **2003**, *225*, 25.
(60) Smith, A. C. H.; Caplinger, E.; Neynaber, R. H.; Rothe, E. W.; Trujillo, S. M. *Phys. Rev.* **1962**, *127*, 1647.
(61) Burnett, T.; Rountree, S. P. *Phys. Rev. A* **1979**, *20*, 1468.
(62) Hwang, W.; Kim, Y. K.; Rudd, M. E. *J. Chem. Phys.* **1996**, *104*, 2956.
(63) Iga, I.; Rao, M. V. V. S.; Srivastava, S. K. *J. Geophys. Res.* **1996**, *101*, 9261.
(64) Kim, Y. B.; Stephan, K.; Märk, E.; Märk, T. D. *J. Chem. Phys.* **1981**, *74*, 6771.
(65) Märk, T. D. *J. Chem. Phys.* **1975**, *63*, 3731.
(66) Seaton, M. J. *Phys. Rev.* **1959**, *113*, 814.
(67) Ainich, A. A. *J. Phys. Chem. Ref. Data* **1993**, *22*, 1469.
(68) Johnsen, R. *J. Mass Spectrom. Ion Processes* **1987**, *81*, 67.
(69) Lieberman, M. A.; Lichtenberg, A. J. *Principles of plasma discharges and materials processing*; John Wiley & Sons: New York, 1994.
(70) Raizar, Yu P. *Physics of gas discharges*; Springer-Verlag: Heidelberg, 1990.
(71) Gordillo-Vazquez, F. J.; Kunc, J. A. *Phys. Rev. E* **1995**, *51*, 6010.
(72) Chapman, B. *Glow Discharge Processes, Sputtering and Plasma Etching*; John Wiley & Sons: New York, 1980.
(73) Braithwaite, N. St. *J. Plasma Sources Sci. Technol.* **2000**, *9*, 517.
(74) Marković, V. Lj.; Gocić, S. R.; Stamenković, S. N.; Petrović, A. Lj.; Radmilović, M. *Eur. Phys. J. Appl. Phys.* **2001**, *14*, 171.
(75) Phelps, A. V.; Petrović, Z. Lj. *Plasma Sources Sci. Technol.* **1999**, *8*, R21.